JOURNAL OF MATERIALS SCIENCE 13 (1978) 2585–2393

Fractography of chemical vapour-deposited Si_3N_4

KOICHI NIIHARA, TOSHIO HIRAI
The Research Institute for Iron, Steel and Other Metals, Tohoku University, Sendai, 980, Japan

The fractography of massive amorphous and crystalline chemical vapour-deposited silicon nitride (Pyrolytic-Si_3N_4) prepared under various deposition conditions using $SiCl_4$, NH_3 and H_2 as the source gases has been carried out at room temperature in order to clarify the relation between fracture surfaces and structural features. For amorphous Py-Si_3N_4, three types of fracture surfaces are observed; i.e. (a) a clean contour-like fracture surface, (b) a contour-like fracture surface including black spots and (c) a cone boundary fracture surface. The fracture mode of the crystalline Py-Si_3N_4 depends greatly on the microstructure. The fracture of fine-grained and low-density Py-Si_3N_4 occurs intergranularly, probably due to the presence of the undetectable amorphous Py-Si_3N_4 between grain boundaries, while the coarse-grained and high-density Py-Si_3N_4 with preferred orientations shows transgranular fracture. The fracture surfaces of massive Py-Si_3N_4 are made in comparison with those of the varieties of Si_3N_4 and SiC.

1. Introduction

Silicon nitride (Si_3N_4) is a valuable engineering material with high temperature applications. Bulk Si_3N_4 is available in the form of reaction-sintered (RS), hot-pressed (HP) or chemical vapour-deposited (CVD, Pyrolytic, Py) bodies [1–4].

In general RS-Si_3N_4 exhibits low strength due to its low density, and HP-Si_3N_4 shows a rapid strength degradation at high temperatures above 800° C due to the presence of glassy phases formed by the reaction of Si_3N_4 and dopants added to achieve a high density in the sintering process [5–8]. However, Py-Si_3N_4, with theoretical density and without any additions, is expected to possess superior mechanical properties to those of RS- and HP-Si_3N_4 at elevated temperatures.

The fracture behaviour and other mechanical properties of ceramics such as Si_3N_4 are closely related to the microstructure, density (porosity) and impurity content [9, 10]. Detailed studies of fracture surfaces, therefore, have been performed on RS- and HP-Si_3N_4 in order to investigate the correlations between the microstructure, strength and fracture mechanisms [5, 8, 11–15]. It has been reported that the fracture occurs transgranularly in high-density Py-SiC [9] and intergranularly in the low density Py-SiC with secondary phases [16], and that the decrease in strength at high temperatures is not observed in the former. Therefore, Py-Si_3N_4 would be expected to have an excellent high-temperature strength if transgranular fracture occurs. However, little is known about the fracture surfaces of Py-Si_3N_4. The object of this paper is to report on the fracture surfaces of Py-Si_3N_4 at room temperature, especially with respect to the relations between fracture surfaces and structural features.

2. Experimental procedures

2.1. Py-Si_3N_4 samples

Amorphous and crystalline samples of Py-Si_3N_4 in the massive form were deposited on a directly-heated graphite substrate using a NH_3–$SiCl_4$–H_2 flow system. Pyrolysis was performed at deposition temperatures (T_{dep}) of 1100 to 1400° C, total gas pressures (P_{tot}) of 10 to 60 Torr, and flow rates of NH_3, 60; $SiCl_4$, 0.8 (in liquid) and H_2, 700 cm^3 min^{-1}. The procedures of sample preparation have been fully described elsewhere [4]. The Py-Si_3N_4 samples used in the present fracture experiments

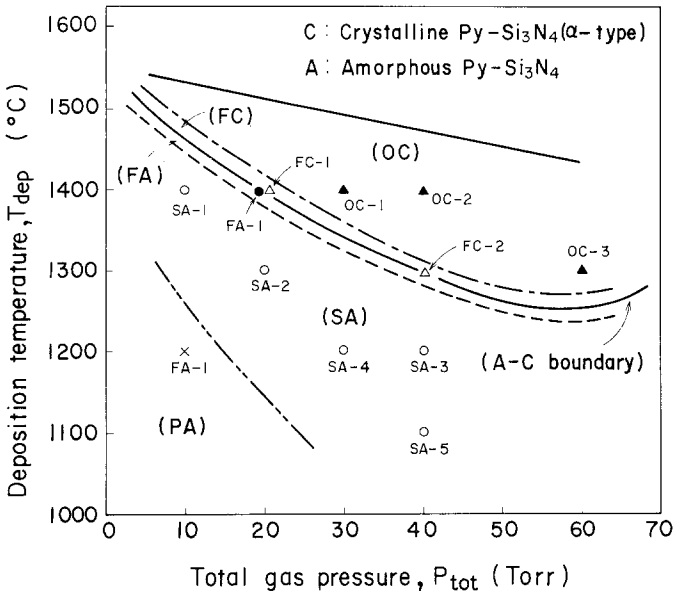

Figure 1 Effect of the deposition temperature (T_{dep}) and the total gas pressure (P_{tot}) on the structure of Py-Si_3N_4. PA: the amorphous deposits with only primary cones; SA: the amorphous deposits with primary and secondary cones; FA: the amorphous deposits with primary and fine secondary cones; FC: the fine grained crystalline deposits with the average grain size ~ 1 μm (α-type), and OC: the preferentially oriented crystalline deposits with the average grain size above 10 μm (α-type).

were prepared under the conditions shown in Fig. 1. Some properties of the samples are summarized in Table I [4, 17, 18].

2.2. Scanning electron microscopic observations

The Py-Si_3N_4 samples with dimensions of 15 mm x 3 mm x (1.8 ~ 2.5) mm were fractured in the growth direction using a three-point bending jig at room temperature. The surfaces of specimens fractured were coated with gold to a thickness of approximately 50 to 100 Å and then examined by a Hitachi–Akashi scanning electron microscope (Type: MSM 4) at magnifications x 100 to x 20 000.

3. Experimental results

3.1. Amorphous Py-Si_3N_4

The fracture surface of the massive amorphous Py-Si_3N_4 may be divided into three types as shown in Figs. 2 to 4, depending upon the microstructure.

Fig. 2 exhibits the as-deposited (a) and fracture (b) surfaces of PA-1. Under high magnifications the fracture surface shows a contour-like surface which is similar to those observed in glassy materials [10]. This is classified as the first typical fracture surface. There is no evidence that the other phases, pores and cracks are included in the deposits. A similar type of fracture surface was also observed for SA-1 and SA-2 with the as-

TABLE I Description of the varieties of Py-Si_3N_4 used in the present experiments

Sample	Crystal structure*	Density ($g\,cm^{-3}$)	Preferred orientation	Cone and grain size (μm)
PA-1	A	2.83	–	30
SA-1	A	2.89	–	10
SA-2	A	2.87	–	15
SA-3	A	2.60	–	15
SA-4	A	2.67	–	13
SA-5	A	2.70	–	10
FA-1	A	2.90	–	7
FC-1	C	3.15	(2 2 2)	7
FC-2	C	3.16	(2 2 2), (1 1 0), (2 1 0)	1
OC-1	C	3.18	(2 2 2)	15
OC-2	C	3.18	(2 2 2)	16
OC-3	C	3.17	(1 1 0), (2 1 0)	10

* A: amorphous; C: crystalline (α-Si_3N_4).

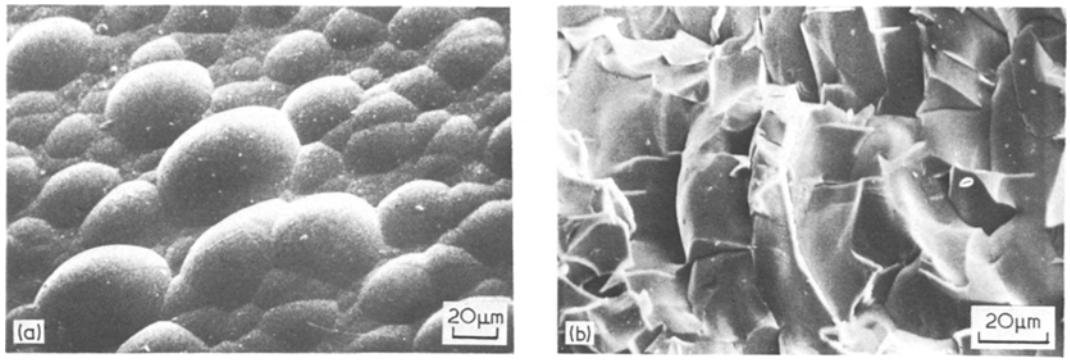

Figure 2 Scanning electron micrographs of (a) as-deposited and (b) fracture surfaces of amorphous Py-Si_3N_4 (PA-1).

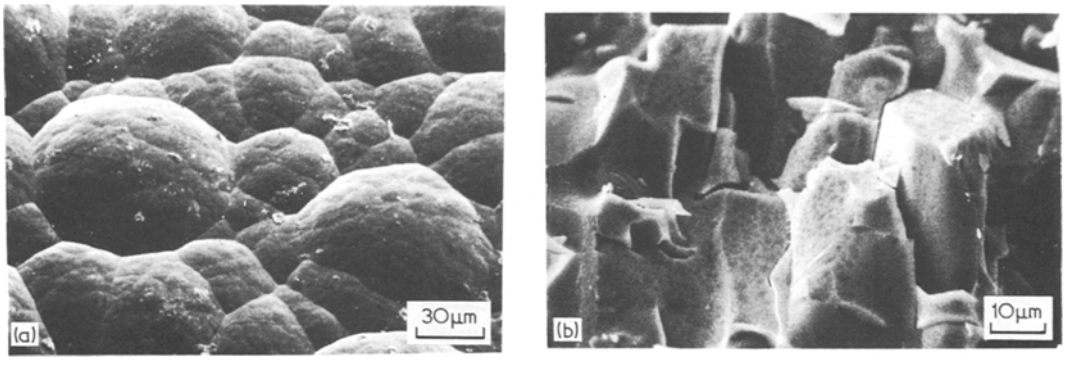

Figure 3 Scanning electron micrographs of (a) as-deposited and (b) fracture surfaces of amorphous Py-Si_3N_4 (SA-3).

deposited surface structure composed of the primary and secondary cones (see Fig. 3a), prepared at high T_{dep} above 1300° C in the SA region shown in Fig. 1.

The second typical fracture surface was observed in the deposits (SA-3, SA-4, SA-5) prepared at T_{dep} below 1200° C in the SA region. The morphology of the as-deposited surfaces is similar to that in Fig. 3a. A second typical fracture surface obtained for SA-3 is shown in Fig. 3b. A large number of black spots exist in the contour-like fracture surface, indicating the presence of secondary phases.

A third typical fracture surface was observed for FA-1 produced in the A–C boundary region shown in Fig. 1. Fig. 4a shows the as-deposited surface of FA-1 in which large primary cones contain a large number of well-defined small secondary cones. As shown in Fig. 4b, the fracture in FA-1 may occur at the large primary cone boundaries.

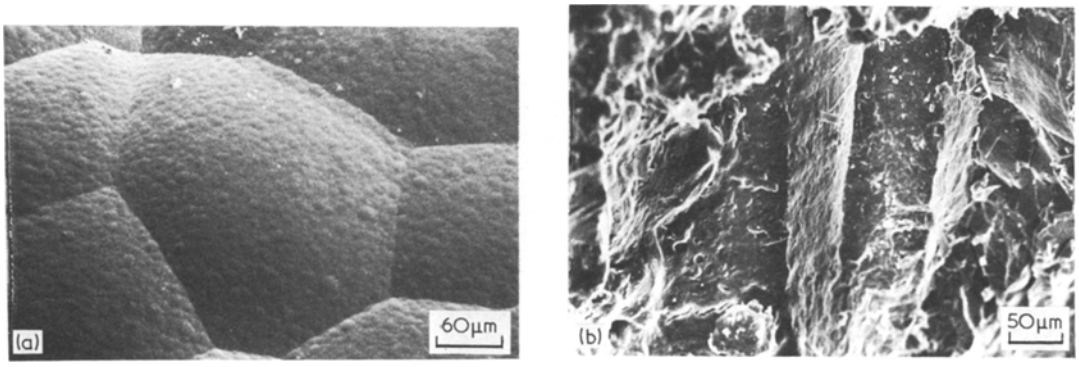

Figure 4 Scanning electron micrographs of (a) as-deposited and (b) fracture surfaces of amorphous Py-Si_3N_4 (FA-1).

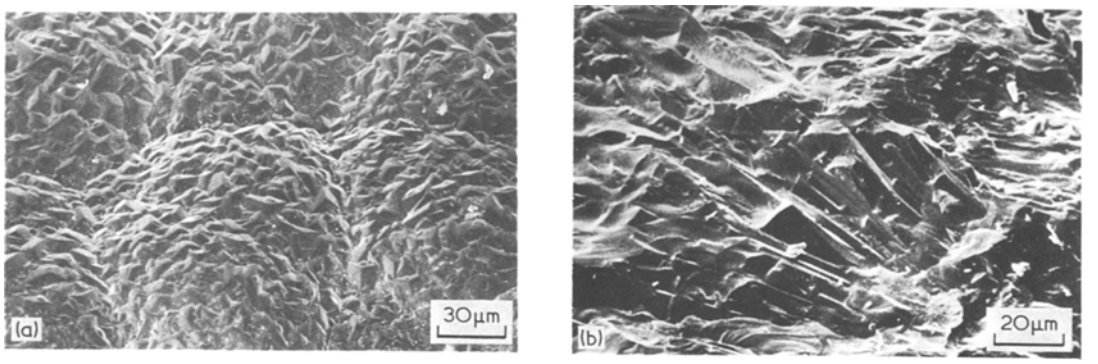

Figure 5 Scanning electron micrographs of (a) as-deposited and (b) fracture surfaces of crystalline Py-Si_3N_4 (FC-1).

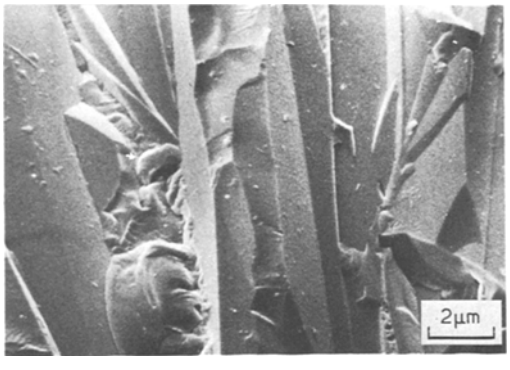

Figure 6 Scanning electron micrograph of the fracture surface of crystalline Py-Si_3N_4 (FC-2).

This fracture behaviour is similar to that of crystalline Py-Si_3N_4, as will be described in Section 3.2.

3.2. Crystalline Py-Si_3N_4

Figs. 5a and b show the as-deposited and fracture surfaces of FC-1 prepared in the A–C boundary region, respectively. This implies that the fracture of FC-1 is predominantly intergranular, although transgranular fracture is also observed. Fig. 6 shows the fracture surface of fine-grained crystalline Py-Si_3N_4 with an average grain size of about 1 μm (FC-2). The fracture of FC-2 seems to be almost entirely intergranular.

The as-deposited and fracture surfaces of OC-1 are shown in Figs. 7a and b, respectively. X-ray diffraction revealed strong (2 2 2) preferred orientations parallel to the deposition surface, and the average grain size was approximately 15 μm [18]. As shown in Fig. 7b, the fracture of OC-1 may be primarily transgranular. A similar fracture surface was also observed in OC-2 with a strong (2 2 2) orientation.

Fig. 8 shows the fracture surface of OC-3 with remarkable (1 1 0) and (2 1 0) orientations. The as-deposited surface of faceted growth can be partly seen in the upper part of Fig. 8. Fracture also occurs in a transgranular mode.

4. Discussion

The fractography of RS- and HP-Si_3N_4 has been made in detail in order to clarify the relation between microstructures and fracture mechanisms

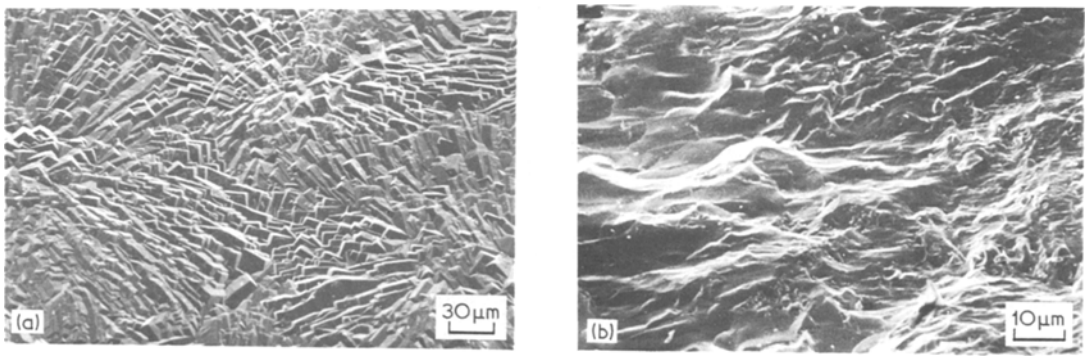

Figure 7 Scanning electron micrographs of (a) as-deposited and (b) fracture surfaces of crystalline Py-Si_3N_4 (OC-1). The deposition surface is to the right of Fig. 7b.

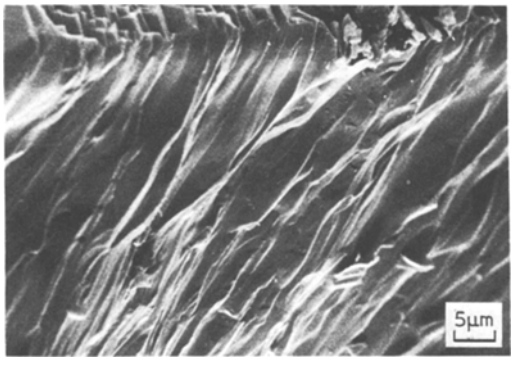

Figure 8 Scanning electron micrograph of the fracture surface of crystalline Py-Si_3N_4 (OC-3).

[5–7, 11–15, 19, 20]. In a study of the fracture resistance of RS-Si_3N_4 at room temperature, Barnby and Taylor [12] found that the crack path in the pure β-Si_3N_4 body was intergranular, while the predominantly α-Si_3N_4 body showed a flatter crack surface where the crack path traversed α needle-like grains.

The relations between microstructure, strength and fracture surface in the different varieties of Si_3N_4 and SiC are summarized in Table II [7, 9, 13–16, 19–29].

In Norton HS-130 of HP-Si_3N_4 containing MgO as the dopant [14], the fracture mode at 77 K is almost transgranular, as shown in Table II. As the temperature is raised, the intergranular fracture is predominant up to 1000° C. Above this temperature only the intergranular fracture is observed. A similar tendency is also observed in Norton HS-110 [19, 20]. On the other hand, it is generally believed that HP-Si_3N_4 with MgO additions, such as Norton HS-130, HS-110 and Lucas HS-110, shows a rapid reduction in strength at temperatures above ~1000° C as a result of softening of the glassy phases existing in the grain boundaries [7, 8, 13, 21]. The temperature at which the fracture is completely intergranular corresponds fairly well to that leading to a rapid reduction in strength. Therefore, in the case of HP-Si_3N_4 containing MgO, the change from the transgranular to the intergranular fracture mode with increase in temperature can be considered to be attributed to the softening of the glassy phases in the grain boundary.

The above relations are also applied to HP-Si_3N_4 with Y_2O_3 additions. Tsuge *et al.* [30] reported that the HP-Si_3N_4 containing the crystalline grain boundary phase $Si_3N_4 \cdot Y_2O_3$ produced quite complex and brittle fracture at 1300° C, whereas HP-Si_3N_4 with glassy phases showed a comparatively smooth fracture surface due to the softening of the glassy phases at that temperature. In the latter case, the three-point bending strength at 1300° C is lower than that of the former, which is probably the result of intergranular fracture.

As shown in Table II, a similar temperature dependence of fracture mode was found in HP-SiC with B and Si_3N_4 additions, NC-201 and NC-203 with Al_2O_3 additions, and self-bonded KT-SiC, which included glassy phases and free Si as secondary phases [13, 21, 23, 24] and showed intergranular fracture. These materials also show a rapid reduction in strength at high temperatures.

Unlike HP-Si_3N_4, HP-SiC and KT-SiC containing glassy phases or free Si as secondary phases, the increase in strength with temperature has been observed in single phase SiC bodies such as sintered SiC with B and C additions, HP-SiC with BN additions [23] and high-density Py-SiC [9]. Similar behaviour was observed for SiC single crystals [31]. All of these materials showed transgranular fracture even at high temperatures.

Although the B-doped HP-SiC contains SiO_2 as a secondary phase, it does not show intergranular fracture [22]. The fracture was reported to be still transgranular even at 1600° C, although a reduction in strength was observed at high temperatures. Unfortunately, it is difficult to assess the reliability of this result, because the examination was carried out after etching away the oxide film from the oxidized fracture surface.

The fracture surface of Py-SiC has been investigated in detail. Ogawa *et al.* [16] reported that the fracture of Py-Sic composed mainly of a β-phase was predominantly intergranular. Gulden [9] found that the fracture mode of the coase-grained and highly dense Py-SiC (β) was transgranular between room temperature and 1400° C, and that the strength increased sharply as temperature was raised above 900° C. However, the fracture mode of fine-grained and low-density Py-SiC containing pores in grain boundaries varies from transgranular at room temperature to intergranular at high temperatures, and the strength decreased slightly at high temperatures.

From the experimental results presented above, the effect of the temperature dependence of the fracture mode on the strength may be

TABLE II Microstructure, strength and fracture mode of the varieties of Si_3N_4 and SiC

Material	Phase*	Dopant	Density ($g\,cm^{-3}$)	Grain morphology	Grain size† (μm)	Four-point bending strength‡ ($kg\,mm^{-2}$)	Fracture mode §	Reference
Hot-pressed Si_3N_4								
HS-110 (Norton)	$\beta + \alpha$ + g	MgO	3.20	equiaxed elongated	1.3	53 (RT) 12 (1400° C)	I (RT) I (1260° C)	[7, 15, 19–21]
HS-130 (Norton)	$\beta + \alpha$ + g	MgO	3.19	equiaxed elongated	1.3	53 (RT) 28 (1400° C)	T (77 K) I (1000 ~ 1400° C)	[7, 14, 15, 19–21]
HS-110 (Lucas)	$\beta + \alpha$ + SiC + C + g	MgO	3.17	angular acicular	0.1 ~ 2	71 (RT) 27 (1400° C)	I (RT) –	[13, 21]
Hot-pressed SiC								
HP-SiC (GE)	$\beta + \alpha + SiO_2$	B	3.19	equiaxed	3.2	[58] (RT) [31] (1600° C)	T (RT) {T} (1600° C)	[22]
HP-SiC (GE)	$\alpha + \beta$ + Si	B + Si_3N_4	3.18	equiaxed	2 ~ 3	72 (RT) 32 (1500° C)	I (RT) I (1500° C)	[23]
HP-SiC (GE)	β	BN	3.13	equiaxed	3	31 (RT) 48 (1500° C)	T (RT) T (1500° C)	[23]
NC-201 (Norton)	α + g	Al_2O_3	3.2	equiaxed	2 ~ 5	58 (RT) 42 (1500° C)	I (RT) I (1200° C)	[13, 21]
NC-203 (Norton)	α + g	Al_2O_3	3.2	equiaxed	0.5 ~ 2	[77] (RT) [32] (1500° C)	I + T (RT) I (high temp)	[21, 24]
Self-bonded SiC								
KT-SiC (Carborundum)	$\alpha + \beta$ + Si	–	3.13	equiaxed bimodal	40 (largest)	18 (RT) 13 (1482° C)	I (RT) I (high temp)	[21, 25–28]
Refel-SiC (UKAEA)	$\alpha + \beta$ + Si	–	3.10	equiaxed	12	42 (RT) 25 (1400° C)	T + I (RT) –	[25, 28, 29]

TABLE II (continued)

Recrystallized SiC								
Crystar-SiC (Norton)	$\alpha + \beta$	–	2.66	equiaxed bimodal	10 (largest)	[18] (RT) [18] (1400° C)	T + I (RT) –	[21, 24, 25]
Sintered SiC (GE)	β	B + C	3.03	equiaxed bimodal	–	35 (RT) 39 (1500° C)	T (RT) T (1500° C)	[23]
Py-SiC								
Py-SiC	β	–	3.21	columnar	~ 15	94 (RT) 133 (1400° C)	T (RT) T (1400° C)	[9]
Py-SiC	β	–	3.17	columnar	~ 4	97 (RT) 89 (1400° C)	T (RT) I (1400° C)	[9]
Py-SiC	$\beta + \alpha$ + Si	–	3.19	dendritic	[200]	~ 65 (RT)	I (RT)	[16]
Py-Si_3N_4								
Py–Si_3N_4	α	–	3.18	columnar	~ 15	–	T (RT)	This work
Py-Si_3N_4	α	–	3.15	columnar	~ 1	–	I (RT)	This work

*α: α-Si_3N_4 or α-SiC; β: β-SiC; g : glassy phase.
†[ ]: crystalline size (Å).
‡RT: room temperature; [ ]: three-point bending strength.
§RT: room temperature; { }: the fracture surface was oxidized; I: intergranular fracture; T: transgranular fracture.

TABLE III Effect of fracture mode on the temperature dependence of strength for the varieties of Si_3N_4 and SiC

Type	Fracture mode*		Strength at	Material	Reference
	Room temperature	High temperature	high temperature		
Type 1	I or I + T	I	Decrease	Poly-phase materials (RS-Si_3N_4, HP-Si_3N_4, KT-SiC, Refel-SiC, Crystar-SiC, NC-201, NC-203, HP-SiC with B or B + Si_3N_4 additions, Py-SiC with intergranular porosity or free Si)	[7, 12–16, 19–29]
Type 2	T	T	Increase	Single phase materials without intergranular porosity (single crystal SiC, sintered SiC with B + C additions, HP-SiC with BN additions, high-density Py-SiC)	[9, 23, 31]

*I: intergranular fracture; T: transgranular fracture.

divided into two types, as summarized in Table III for Si_3N_4 and SiC bodies.

The fracture mode of massive crystalline Py-Si_3N_4 in the present experiments depended strongly upon microstructure. The intergranular fracture mode was mainly observed for the fine-grained and low-density Py-Si_3N_4 prepared in the A–C boundary region (FC-1, FC-2, see Figs. 5b and 6). This observation is similar to the result of Ogawa *et al.* [16] on Py-SiC, probably due to the trace of undetectable amorphous Py-Si_3N_4 contained in grain boundaries of the crystalline Py-Si_3N_4. On the other hand, the coase-grained and high-density Py-Si_3N_4 prepared in the OC region showed transgranular fracture, as expected from the theoretical density (free pores) and high purity (OC-1, OC-2, OC-3, see Figs. 7b and 8). This behaviour seems to be similar to that of the coase-grained and highly dense Py-SiC reported by Gulden [9].

The number of spots that characterizes the second typical fracture surface of the massive amorphous Py-Si_3N_4 (see Fig. 3b) decreases with increasing density. The spots were not identified in PA-1, SA-1 and SA-2 with a density in excess of 2.80 g cm^{-3}. Thus, it is reasonable to consider that the structure in the spots is different from that in the matrix of amorphous Py-Si_3N_4. Various complex intermediates can be produced during a pyrolysis of a $SiCl_4$–NH_3 system: $Si(NH)_2$, $[Si_3(NH)_3N_2]_n$, $[Si_2(NH)N_2]_n$, $Si_3N_5H_3$ and Si_2N_3H [32–34]. The Si–H bond in the Si–N–H intermediates is relatively stable at 1050 to 1400° C, although its stability depends strongly upon the intitial reaction temperature between $SiCl_4$ and NH_3 [34]. Moreover, the oxygen content in SA-3 is known to be about 2 wt% [4]. Therefore, the spots might be related to the intermediates in the Si–N–H, Si–N–O or Si–N–O–H systems.

Acknowledgements

This research was supported in part by a scientific research fund from the Ministry of Education, Contract Nos. 047015 and 285168.

References

1. N. L. PARR and E. R. W. MAY, *Proc. Brit. Ceram. Soc.* 7 (1967) 81.
2. R. F. COE, R. J. LUMBY and M. F. PAWSON, "Special Ceramics 5", edited by P. Popper (British Ceramic Research Association, Stoke-on-Trent, 1972) p.361.
3. F. GALASSO, U. KUNTZ and W. J. CROFT, *J. Amer. Ceram. Soc.* 55 (1972) 431.
4. K. NIIHARA and T. HIRAI, *J. Mater. Sci.* 11 (1976) 593.
5. A. G. EVANS and R. W. DAVIDGE, *ibid.* 6 (1971) 1292.
6. B. F. JONES and M. W. LINDLEY, *ibid.* 11 (1976) 1288.
7. F. F. LANGE, *J. Amer. Ceram. Soc.* 57 (1974) 84.
8. S. WILD, P. GRIEVESON, K. H. JACK and M. LATIMER, "Special Ceramics 5", edited by P. Popper (British Ceramic Research Association, Stoke-on-Trent, 1972) p. 377.
9. T. D. GULDEN, *J. Amer. Ceram. Soc.* 52 (1969) 585.

10. H. CONRAD and E. STOFEL, "Modern Ceramics", edited by J. E. Hove and W. C. Riley (John Wiley, New York, 1965) p. 133.
11. B. J. DALGLEISH and P. L. PRATT, *Proc. Brit. Ceram. Soc.* **22** (1973) 323.
12. J. T. BARNBY and R. A. TAYLOR "Special Ceramics 5", edited by P. Popper (British Ceramic Research Association, Stoke-on-Trent, 1972) p. 311.
13. W. ASHCROFT, "Special Ceramics 6", edited by P. Popper (British Ceramic Research Association, Stoke-on-Trent, 1975) p. 245.
14. J. L. HENSHALL, D. J. ROWCLIFFE and J. W. EDINGTON, *ibid.* p. 245.
15. R. KOSSOWSKY, *J. Mater. Sci.* 8 (1973) 1603.
16. K. OGAWA, K. FUKUDA and K. IWAMOTO, *ibid.* **11** (1976) 1362.
17. K. NIIHARA and T. HIRAI, *ibid.* **11** (1976) 604.
18. *Idem, ibid.* **12** (1977) 1233.
19. R. KOSSOWSKY, D. G. MILLER and E. S. DIAZ, *ibid.* **10** (1975) 983.
20. R. KOSSOWSKY, "Ceramics for High-Performance Applications", edited by J. J. Burke, A. E. Gorum and R. N. Katz (Brook Hill, Massachusetts, 1974) p. 347.
21. J. W. EDINGTON, D. J. ROWCLIFFE and J. L. HENSHALL, *Powder Met. Int.* **7** (1975) 82.
22. S. PROCHAZKA and R. J. CHARLES, *Bull. Amer. Ceram. Soc.* **52** (1973) 885.
23. S. PROCHAZKA and P. C. SMITH, Final Report SDR-74-040 Contract N62269-73-C-0356 (1973).
24. M. L. TORTI, *Powder Met. Int.* **6** (1974) 186.
25. G. Q. WEAVER, H. R. BAUMGARTNER and M. L. TORTI, "Special Ceramics 6", edited by P. Popper (British Ceramic Research Association, Stoke-on-Trent, 1975) p. 261.
26. Carborundum Co. Data Sheet.
28. R. STEVENS, *J. Mater. Sci.* **6** (1971) 324.
29. C. W. FORREST, P. KENNEDY and J. V. SHENNAN, "Special Ceramics 5", edited by P. Popper (British Ceramic Research Association, Stoke-on-Trent, 1972) p. 99.
30. A. TSUGE, K. NISHIDA and M. KOMATSU, *J. Amer. Ceram. Soc.* **58** (1975) 323.
31. D. P. H. HASSELMAN and H. D. BATHA, *Appl. Phys. Lett.* **2** (1963) 111.
32. O. GLEMSER and P. NAUMANN, *Z. Anorg. Allgem. Chem.* **298** (1958) 134.
33. K. S. MAZDIYASNI and C. M. COOKE, *J. Amer. Ceram. Soc.* **56** (1973) 628.
34. A. KATO, Y. ONO, S. KAWAZOE and L. MOCHIDA, *Yogyo-Kyokai-Shi* **80** (1972) 28.

Received 20 January and accepted 10 March 1978.